

Document image classification, with a specific view on applications of patent images*

Gabriela Csurka

*Xerox Research Centre Europe, 6 chemin de Maupertuis
38240, Meylan France
Firstname.Lastname@xrce.xerox.com*

January 14, 2016

Abstract

The main focus of this paper is document image classification and retrieval, where we analyze and compare different parameters for the RunLength Histogram (RL) and Fisher Vector (FV) based image representations. We do an exhaustive experimental study using different document image datasets, including the MARG benchmarks, two datasets built on customer data and the images from the Patent Image Classification task of the Clef-IP 2011. The aim of the study is to give guidelines on how to best choose the parameters such that the same features perform well on different tasks. As an example of such need, we describe the Image-based Patent Retrieval task's of Clef-IP 2011, where we used the same image representation to predict the image type and retrieve relevant patents.

1 Introduction

“Before a patent can be granted, patent offices perform thorough searches to ensure that no previous similar disclosures were made. In the intellectual property terminology, such kind of searches are called prior art searches [...] Often, patent applications contain images that clarify details about the invention they describe. Images in patents may be drawn by hand, by computer, or both, may contain text, and are generally black-and-white (i.e. not even monochrome). Depending on the technological area of a patent, images may be technical drawings of a mechanical component, or an electric component, flowcharts if the patent describes, for example, a workflow, chemical structures, tables, etc. When a patent expert browses through a list of search results given by a search engine, he or she can very quickly dismiss irrelevant patents to the patent application by just glancing at the images in the retrieved patents. The number of documents to be looked at in more detail is thus greatly reduced.” [30].

From this citation we can see that images are essential components of a patent as they illustrate key aspects of the invention. However, not every image in a patent has

*To appear in M. Lupu *et al.* (eds.), Current Challenges in Patent Information Retrieval, second edition, 2016. Paper submitted in 2014.

the same importance. Indeed, for patents related to chemistry or to pharmaceutic inventions images containing chemical structures or gene sequences are the most important, while searching for similar drawings containing electronic circuits can help patent experts in physics and electricity. If a patent expert is looking for prior art given a query patent and the system retrieves patent based on visual similarities between all images of the query patent and in the patent database, the system might return non relevant patents based on visual similarity between flowcharts or tables. This would not necessarily help the prior art search process. On contrary, if only images of a certain type are considered, the retrieval can be significantly improved as shown in [11] where the retrieval accuracy when searching for the most similar drawings between patent images was much higher than the accuracy obtained when considering similarities between all images. However this requires first to identify the image type (such as drawing, flowchart, ...) to be considered.

In general manual annotation of the patent images according to their type is either non-existent or poor with many errors, therefore there is a clear need to be able to predict the image type automatically. Hence, one of the main focus of this paper is to consider patent image classification according to image types as the ones identified and used in the Patent Image Classification task of Clef-IP 2011 [30], namely *abstract drawing, graph, flowchart, gene sequence, program listing, symbol, chemical structure, table and mathematics*. On the other hand, as similar image search (retrieval) is another important aspect of patent based applications such as prior art search, in the paper we also address image similarities and image based retrieval. For both tasks, we consider mainly two popular image representations, the Fisher Vector [27, 29] and the RunLengths Histograms [8, 22, 15, 18], and compare different parameter configurations for them in order to come with useful guidelines related to their choice independently of the targeted problem.

As patent images can be seen as particular document images, instead of limiting our study to patent images, we will address the problem in a more generic way, by questioning what is a good representation in general for document images. First, in section 2 we briefly revise the most popular document image representations. Then, after describing in section 3 the datasets considered for the study and the experimental setup, section 4.1 and section 4.2 will be devoted to an exhaustive parameter comparison for RunLength and Fisher Vector image representations respectively and in section 4.3 we discuss different combinations of RL and FV. In section 5 we we describe the Image-based Patent Retrieval task's of Clef-IP 2011, where we used the same image representation to predict the image type and retrieve relevant patents. Finally, we conclude the paper in section 6.

2 Document Image Representations

In the last few years different image representations were proposed to deal with document image classification and retrieval that do not rely on OCR *i.e.* seeing a document page as an image. To mention a few, see for more examples [9, 22, 15], Cullen *et al.* [12] propose feature sets including densities of interest points, histogram of the size and density of connected components, vertical projection histograms etc. In [20] a multi-scale density decomposition of the page is used to produce fixed-length descriptors constructed efficiently from integral images. The features vectors proposed in [35] are based on text versus non-text percentage, column structure, content area and connected components densities. Bagdanov and Worring [5] propose a representation

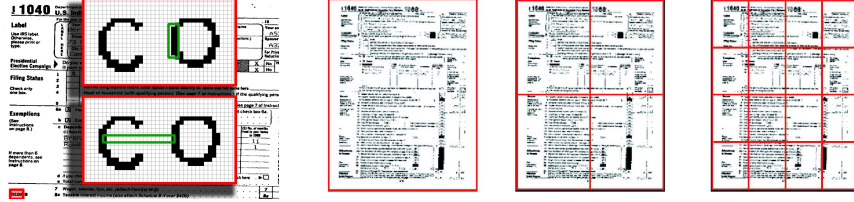


Figure 1: Left: Examples of pixel runs. A vertical black run of length 7 (top) and an horizontal white run of length 16 (bottom). Detail from a small region on the bottom-left corner. Right: A tree layer spatial pyramid. (Image courtesy of A. Gordo, from [15]).

based on density changes obtained with different morphological operations. In [34] document images are described as a list of salient Viola-Jones based features. However, these features contain relatively limited amount of information and while they might perform well on a specific dataset and task for which they were designed, they are not generic enough to be able to handle various document class types, datasets and tasks. As early natural image representations, such as color histograms, were significantly outperformed and replaced by the successful introduction of the bag of visual words (BOV) image representation [36, 10], the RunLength Histograms have shown to be more generic and hence better suited for document image representation¹ [8, 22, 15, 18].

In this work, therefore we focus on one hand on the RunLength Histograms, on the other hand we consider as alternative the Fisher Vectors [27, 29] which is the most successful extension of BOV image representation. In the following sections we briefly describe how these features are extracted from a document image and which are their main parameters that have to be considered in particular when we build the corresponding image signatures.

2.1 RunLength Histogram based Document Image Representation

The main idea of the RunLength (RL) features is to encode sequences of pixels having the same value and going in the same direction (*e.g.* vertical, horizontal or diagonal). The "run-length" is the length of those sequences (see as examples the green rectangles in the Fig.1). While we can consider sequences of similar gray-scale or even color values, considering only two levels has been proved to be sufficient to characterize document images [15, 18]. Therefore, when needed, we first binarize the document images and we consider only runs of black and white pixels. In case of color images, the luminance channel is binarized.

To do the binarization, we do a simple thresholding at 0.5 (where image pixels intensities are represented between 0 and 1). More complex binarization techniques exist (see for example methods that participated in the DIBCO [31] and HDIBCO [31] contests), however testing the effect of different binarization techniques is out of the scope of this paper.

On the binarized images, the number of black pixel and white pixel runs are collected into histograms. To build these histograms, with the aim of being less sensitive

¹Note that since when the paper was written, with the recent success of the deep convolutional neural networks (CNNs), new, richer representations were proposed for natural images and applied also to document images [21, 19]. The comparison of those representations with FV and RL is subject of future work.

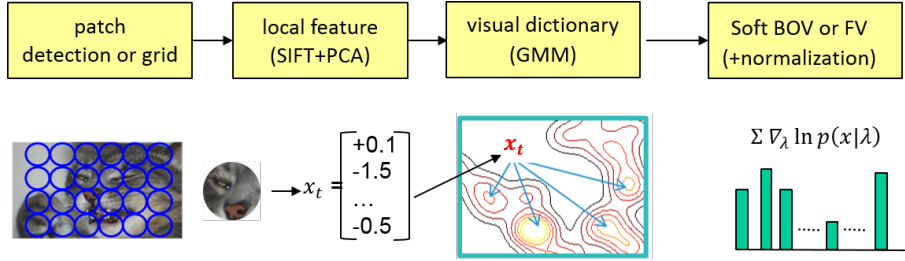


Figure 2: Illustration of the FV image representation pipeline.

to noises and small variations, we consider logarithmic quantization of the lengths as suggested in [15, 18]:

$$[1], [2], [3-4], [5-8], [9-16], \dots, [\geq (2^q + 1)].$$

Dealing with binary images, this yields 2 histograms of length $Q = q + 2$ per direction, one for the white pixels and one for the black pixels. We compute these runs in 4 directions, horizontal, vertical, diagonal and anti-diagonal, and concatenate the obtained histograms. An image (or image region) is then represented by this $4 \times 2 \times Q$ dimensional feature called RunLength (RL) histogram.

These histograms can be computed either on the whole image or on image regions. In order to better capture information about the page layout we use a spatial pyramid [24] with several layers such that at each level the image is divided into $n \times n$ regions and the histograms computed on these regions are concatenated. For example, in the case of a 3 layer pyramid $1 \times 1, 2 \times 2, 4 \times 4$ illustrated in Fig.1(right), we concatenate in total the RLs of 21 regions to obtain the final image signature.

Finally, to be independent from the image size (number of pixel in the image) we L1 normalize the signature followed by a component-wise power normalization² with $\alpha = 0.5$ as in [18]. Note that a vector with positive elements having L1 norm equal to 1, after power normalization will have L2 norm equal to 1.

2.2 The Fisher Vector based Image representation

The Fisher Vector [27] extends the bag-of-visual words (BOV) image representation by going beyond simple counting (0-order statistics) as they encode higher order statistics about the distribution of local descriptors assigned to visual words (see also Fig.2 illustrating the pipeline). Similarly to the BOV, the FV depends on an intermediate representation: the visual vocabulary [36, 10]. The visual vocabulary can be seen as a probability density function (pdf) which models the emission of the low-level descriptors in the image. In our case we consider the Gaussian mixture model (GMM) to represent this density.

The Fisher Vector characterizes the set of low-level features (in our case SIFT features [25]), $X_I = \{\mathbf{x}_I\}_{I=1}^T$ extracted from an image I by deriving in which direction the parameters of the GMM model should be modified to best fit this particular feature set.

²The component-wise power normalization [29] of a vector is such that each element z is replaced by $\text{sign}(z)|z|^\alpha$.

Assuming independence, this can be written as:

$$G_\lambda(I) = \frac{1}{T} \sum_{t=1}^T \nabla_\lambda \log \left\{ \sum_{n=1}^N w_n \mathcal{N}(\mathbf{x}_t | \mu_n, \Sigma_n) \right\} \quad (1)$$

where w_n , μ_n and Σ_n denote respectively the weight, mean vector and covariance matrix of the Gaussian n and N is the number of Gaussians in the mixture. To compare two images I and J , a natural kernel on these gradients is the Fisher Kernel $K(I, J) = G_\lambda(I)^\top F_\lambda^{-1} G_\lambda(J)$, where F_λ is the Fisher Information Matrix. As F_λ^{-1} is symmetric and positive definite, it has a Cholesky decomposition $L_\lambda^\top L_\lambda$ and $K(I, J)$ can be rewritten as a dot-product between normalized vectors Γ_λ where:

$$\Gamma_\lambda(I) = L_\lambda G_\lambda(I) \quad (2)$$

to which we refer as the *Fisher Vector* (FV) of the image I .

Following [27, 29] where the covariance matrices in the GMM are assumed to be diagonal and using a diagonal closed-form approximation of F_λ , we have:

$$\Gamma_{\mu_n^d}(I) = \frac{1}{T \sqrt{w_n}} \sum_{t=1}^T \gamma_n(\mathbf{x}_t) \left(\frac{\mathbf{x}_t^d - \mu_n^d}{\sigma_n^d} \right), \quad (3)$$

$$\Gamma_{\sigma_n^d}(I) = \frac{1}{T \sqrt{2w_n}} \sum_{t=1}^T \gamma_n(\mathbf{x}_t) \left[\frac{(\mathbf{x}_t^d - \mu_n^d)^2}{(\sigma_n^d)^2} - 1 \right] \quad (4)$$

where $\gamma_n(\mathbf{x}_t) = \frac{w_n \mathcal{N}(\mathbf{x}_t | \mu_n, \Sigma_n)}{\sum_{j=1}^N w_j \mathcal{N}(\mathbf{x}_t | \mu_j, \Sigma_j)}$ and σ_n^d are the elements of the diagonal Σ_n . The final gradient vector $\Gamma_\lambda(I)$ is the concatenation of all $\Gamma_{\mu_n^d}(I)$ and $\Gamma_{\sigma_n^d}(I)$, where we ignore the gradients with respect to the weights. This vector is hence $2ND$ -dimensional, where D is the dimension of the low level features \mathbf{x}_t .

As proposed in [29] we further apply on $\Gamma_\lambda(I)$ a component-wise power normalization a component-wise power normalization [29], followed by L2 normalization. Finally, similarly to the RunLength features, to better take into account the document layout, we also consider similar spatial pyramids [24] as in the case of RLs, *i.e.* dividing the image into several regions at multiple layers and concatenating the region FVs.

3 Datasets and the experimental setup

We used the following document image datasets³ in our experiments (see examples in Fig.3-4 and statistics in Table 1):

MARG is the Medical Article Records Ground-truth (MARG) dataset [1] that consists of 1,553 documents, each document corresponding to the first pages of medical journals and their size is of 8.4M. The dataset is divided in 9 different layout types. Surprisingly the number of columns that varied from 1 to 3 within the classes is considered not relevant to distinguish between classes, which makes the dataset challenging as the “visual” similarity is strongly influenced by the number of columns. The

³We also considered the NIST Forms dataset [2], with 20 different classes of tax forms, but as the results on this dataset were often of 100% accuracy, these results were not interesting from a parameter comparison study point of view.

Dataset	NbIm	ImSize	NbCls	Example classes
MARG	1553	8.4	9	typeA, typeB
IH1	11252	3-4M	14	invoices, contracts, ID cards,
NIT	885	5.6M	19	invoices, mails, tables, maps
CLEF-IP	38081	1.5K - 4.5M	9	drawing, graph, flowchart

Table 1: A summary of the dataset statistics

criteria of the ground truth labeling is only the relative position of the title, authors, affiliation, abstract and the text (see for more details <http://marg.nlm.nih.gov/gtdefinition.asp>).

IH1 is the dataset used in [15] that contains 11,252 scanned documents from 14 different document types (categories) such as invoices, contracts, IDs, coupons, etc. The images were obtained by scanning paper documents and their size varies according to the size of the original paper document, most of them however having around 3-4M pixels.

NIT is another in-house dataset of 885 multi-page documents with in total 1809 pages of 5.6M pixels, but we only considered the first page to represent the document⁴. The categories represents as in IH1, document types including invoices, mails, tables, maps, etc, but these documents were not scanned but captured in the print flow and converted to images by the print driver (using the Page Description Languages). Within this dataset the amount of elements per class varies a lot, with several classes having only a few examples, while other classes containing a large percentage of all documents. We have a second dataset similar to NIT but independent from, that we call **XRCE** as the documents were captured in our own print flow. This dataset containing mainly scientific articles, patent applications, reports, tables, mails, etc was used to tune the parameters for some of our parametric models such as SVM or metric learning that were after applied to all the other datasets.

CLEF-IP: contains the training image set from the Patent Image Classification task of the Clef-IP 2011 [11]. The aim of the task in the challenge was to categorize patent images into 9 predefined categories such as abstract drawing, graph, flowchart, gene sequence, program listing, symbol, chemical structure, table and mathematics (see examples in Figure 4). The dataset contains between 300 and 6000 labeled images for each class, in total 38081 images with their resolution varying from 1500 pixels to more than 4.5M pixels.

3.1 The experimental setup and evaluation methods

We randomly split these datasets into train (50%) and test (50%) sets five times and the same splits are kept along all experiments, allowing a comparison between different features, algorithms and parameter settings.

The aim of our experiments is mainly to compare different image representations and to design best practices how to choose the parameters for these representations, preferably, independently of the task. Indeed, while the choice of best parameters can be very dependent on the task, with the increasing amount of data it can be more convenient sometimes to have these features precomputed and pre-stored that allow

⁴We did experiments with multiple pages where we averaged either the signatures, the similarity scores or classification scores, but using only the first page was most often close to best performance.

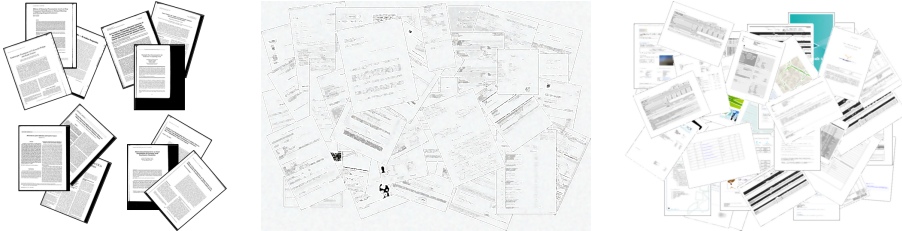


Figure 3: Example images from four MARG class (left), and from the customer datasets IH1 (middle) and NIT (right). The images from customer datasets were intentionally blurred to keep the actual content of the documents confidential. Nevertheless, we can see the visual variability of the documents within these datasets.

using the same representations in various applications such as retrieval, clustering or categorization. Also, as we already mentioned, for image type dependent patent search where the images are first classified, it can be practical to use the same features both for the class prediction and for similar image search.

Our intent therefore is to find feature configurations that perform relatively well across tasks and if possible across datasets. Hence, we evaluate each representation both in a retrieval framework and using different classifiers (SVM, KNN, NCM) and we study the behavior of different parameter configurations. Note that the Nearest Class Mean (NCM) classifier [26] that predicts the class label of a document image based on the closest class mean, evaluates implicitly (in a certain sense) the ability of these features to perform clustering. Indeed, NCM, averaging the examples from each class performs well when these instances can be easily grouped together. Hence a feature configurations yielding better NCM accuracies is more suitable for clustering purposes than one that fails to do it. Further advantages of the NCM are that it is a multi-class classifier and that there is no parameter to be tuned.

When using SVM we used a fixed over all datasets and configurations, which means obviously that the SVM results are sub-optimal (in some cases 1-3to fine tuned parameters). But in some sense this makes the comparison between parametric and non-parametric methods such as NCM fairer. Also the focus of the paper is on the parameters of the image representation and fine tuning the parameters of different classifiers or to test more complex classification methods was out of the scope of the paper. To choose the fixed parameter set for the SVM we tested all configurations and a large set of parameters on the XRCE dataset and considered the setting that performed in general best. As we used one-versus-all linear classifiers with stochastic gradient descend [7] shown to be highly competitive when applied on FVs [4], the selected parameters were as follows. We used hinge loss with fixed learning rate $\lambda = 1e - 5$ for RL features and $\lambda = 1e - 4$ for FV. To handle the dataset bias, we weighted the positives by a factor of $\rho = 5$ and to optimize the classifier we updated the gradient by passing $N_i = 100$ times randomly through the whole training set. Similarly, for the same reasons, in the case of the KNN classifier we used a fixed $k = 4$ as it performed the best on XRCE, but again the results are sub-optimal $k = 4$ might vary along different datasets and configurations.

To evaluate the classification tasks using any of the above mentioned classifiers (NCM, KNN and SVM) we show only the overall prediction accuracy (OA), *i.e.* the ratio of correctly predicted document images, but similar behavior was observed when

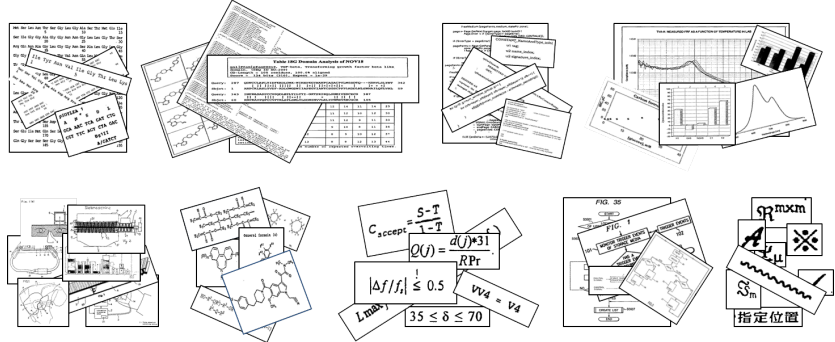


Figure 4: Examples from different classes in the CLEF-IP dataset.

we considered the average of the per class accuracies⁵.

To perform document ranking for the retrieval, we use each test document as query and the aim is to retrieve all documents with the same class label in the training set. As similarity between documents we consider the dot product between features (which is equivalent with the cosine similarity as our features are L2 normalized). To asses the retrieval performance, we use mean average precision (MAP), but we also consider top retrieval accuracy by assessing it by precision at 5 (P@5) as several classes in these datasets have only few representatives. We also consider the precision at 1 (P@1) because this is equivalent with the overall classification accuracy of a KNN classifier using $k=1$ and hence allows us to compare the results with our actual KNN results for which we used $k=4$.

4 Experimental Results

In this section we fist do an exhaustive parameter study for RunLengths in section 4.1 and for Fisher Vectors section 4.2 analyzing the behavior of the parameter configurations considering the previously mentioned tasks and datasets. Then, in section 4.3 we discuss about possibilities how to merge RL with FV.

4.1 Test different parameters for RL

To build different RunLength (RL) features, we mainly varied the image resolution (S), the number of layers⁶ (L) used in the spatial pyramid and the number of quantization bins (Q). When we resize an image, we keep the aspect ratio and we define a maximum resolution. We experimented with target resolutions of 50K, 100K, 250K, 500K and 1M pixels and denoted them by S1, S2, S3, S4 and S5 respectively. In addition, the case where we do not rescale any of the images will be denoted by S0. However, images having less pixels are not upscaled, only images above the target size are downsampled.

In Table 2, we show retrieval performances⁷ (MAP) as well as overall the accuracy

⁵Or when the behavior was different such as for NIT, the reason was that this dataset contains several classes with only few instances meaning that changing the prediction for any of those rare documents may yield a significant change on the accuracy of the corresponding class.

⁶Note that we used 2x2 split of the image at the second layer, 4x4 at the third, 6x6 at the fourth and 8x8 at the fifth. Ln means that we concatenated the features of the regions from all the n layers.

⁷We also assess P@1 and P@5 but show only the MAP here.

	MARG	IH1	NIT	CLEF-IP
MAP	33.8 \pm 1.4 S5,L4,Q11	67.5 \pm 0.5 S5,L1,Q10	42.3 \pm 1.4 S1,L5,Q11	38.3 \pm 0.1 S1,L4,Q7
S	S5 (96/1)	S5 (76/.7)	S1 (96/1)	S2 (56/3)
L	L5 (80/2)	L1 (88/1)	L5 (100/.7)	L5 (60/2)
Q	Q10 (28/.1)	Q7 (32/.2)	Q11 (56/.2)	Q11 (65/.9)
KNN	90.3 \pm 1.6 S0,L5,Q10	95.2 \pm 0.2 S5,L1,Q9	81.3 \pm 1.5 S5,L5,Q10	84.9 \pm 0.2 S0,L1,Q7
S	S5 (60/3)	S0 (56/.4)	S5 (58/2)	S2 (59/1)
L	L5 (87/5)	L1 (74/.7)	L5 (62/3)	L1 (100/3)
Q	Q11 (22/.7)	Q7 (26/.1)	Q9 (27/.6)	Q9 (76/2)
NCM	61.8 \pm 1.5 S0,L5,Q11	91.3 \pm 0.3 S0,L5,Q11	66.6 \pm 0.6 S1,L5,Q10	62.4 \pm 0.2 S0,L3,Q11
S	S0 (38/3)	S0 (67/.8)	S1 (54/2)	S0 (83/3)
L	L5 (80/8)	L5 (60/4)	L5 (98/9)	L4 (50/5)
Q	Q11 (35/1)	Q11 (48/.5)	Q10 (34/1)	Q11 (69/2)
SVM	91.9 \pm 1 S0,L5,Q10	96.9 \pm 0.3 S0,L5,Q11	78.2 \pm 1.2 S5,L5,Q10	89.8 \pm 0.2 S0,L5,Q11
S	S0 (35/4)	S1 (72/.6)	S5 (35/2.5)	S0 (71/2)
L	L5 (67/14)	L5 (65/4)	L5 (72/5)	L4 (52/4)
Q	Q11 (31/3)	Q11 (57/.6)	Q10 (31/.9)	Q11 (66/2)

Table 2: Comparative retrieval (MAP) and classification (KNN, NCM, SVM) results where we vary the parameters of the RL features. We show best results in red (averaged over 5 splits) with the corresponding configuration in blue (below the accuracy), best parameter frequencies nd performance variations best parameter frequencies and performance variations per feature type.

of class prediction (OA) for KNN, NCM and SVM classification. As we mentioned, the experiments were performed on 5 different splits, hence in the table we show the mean over the splits and its variation. For each dataset and task, in addition to the best average, we show, below the best average, the parameter sets that allowed to obtain these results.

In addition, for each parameter type, *e.g.* the number of layer L, we alternatively fix the other parameters, here S and Q, and evaluate the best performing value. We do this for all (S,Q) pairs and retain the corresponding variation. Then, for each value of the selected parameter type, in this example each Li, we compute the percentage of time it performed the best. In Table 2 we show for each parameter type the value (*e.g.* Li) that was found the most often as best performing. In the parenthesis following the parameter found we show two numbers. The first one is the percentage of time that parameter was at the top, the second value shows the average variance of the results for that parameter type (L). This variation was considered by fixing S and Q and evaluating the variance of the results when we varied L, and then averaging over all (S,Q) pairs. These statistics (frequencies and the variance) were computed by cumulating the results along all the 5 splits. Note that if this average variance is low, it means that varying that parameter has relatively low effect on the obtained accuracy, while high average variance means that it is very important to correctly set the given parameter. For example, when we evaluate MARG with MAP we find that L5 performed the best 80% of the time considering all (S,Q) pairs and all splits, and the average variation

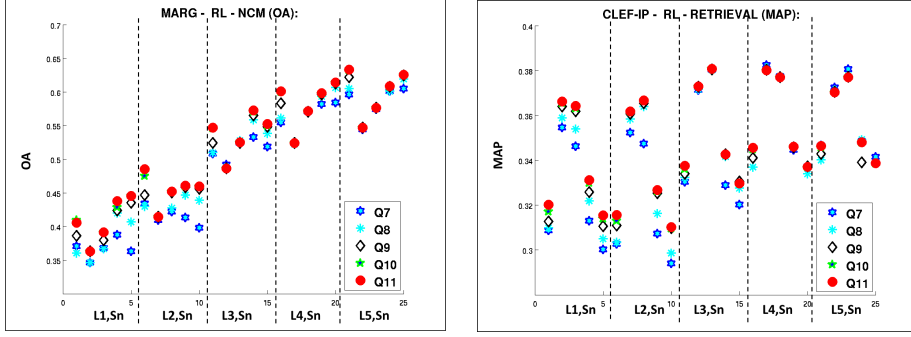


Figure 5: Example plots comparing different quantizations.

along L when fixing (S,Q) was about 2%. This means that setting the number of layers is more important than the choice of the number of quantization bin, as Q10 was best only 28% of times and the average variation of Q when fixing (L,S) was only 0.1%.

When we analyze the values in Table 2, we can deduce the followings:

- Quantization intervals. First of all, we can clearly see that concerning the number of quantization intervals, Q11 is almost always the best option. This shows that considering more quantization values is a good choice. On the other hand, the standard deviation and frequency values are relatively low, which means that the difference with values obtained using fewer quantization intervals (Q7 to Q10) is relatively small, especially when we have best configurations selected for the other parameters (see examples⁸ in Figure 5).

- Number of pyramid layers. We observe that for certain datasets such as MARG or NIT considering multiple layers (L4 or L5) is essential. This is not surprising as the MARG classes are strongly related to the text layout that is much better captured with multiple layers. For other datasets, the best layer configuration seems to be task and evaluation measure dependent (see examples in Figure 6). Indeed, for IH1 and clefIP, top retrieval results and KNN classification perform much better using only a single layer, while MAP, NCM and SVM results are always better with multiple layers (except the MAP for IH1). The main reason is that in the former case, the decision depends only on a few "most similar" documents, hence it is sufficient to have a few similar documents for most instances in the dataset. High KNN values (and top retrieval results, not shown) seems to confirm this for all datasets.

On the contrary, the NCM classifier considers class centroids (*i.e.* averaging over all examples within a class). Therefore for each test example, it is not any more sufficient the presence of a few similar instances but the similarity to most documents within the class becomes necessary. The MAP evaluates how well all instances of a class can be retrieved using an exemplary from the class, which requires again that the within class similarities to be higher than the similarities between instances from other classes. As the NCM and MAP results show, these requirements seems to be better satisfied when we consider multiple layers.

- Image size. Finally, when we try to observe the effect of image resizing, it is

⁸All illustrations plot results from the experiments done on the first split.

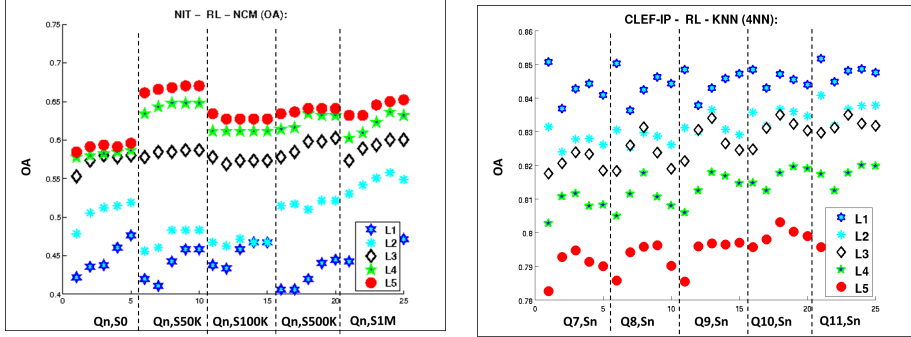


Figure 6: Example images comparing different number of layers.

difficult to draw any interesting conclusions. Best performing image sizes seem to vary along the datasets, tasks and evaluation measures. In a sense, this is not completely surprising, as on one hand the original image sizes vary along datasets. Furthermore, while the size of the RL does not depend on the image size, the distribution of black and white pixel runs within bins is highly correlated with the considered image size. Nevertheless, it seems that S0 appears often as best performing or yields close to best performance as we can see in Figure 7. The advantage of keeping the original size is to preserve the details present in the image as they were captured, but on other hand smoothing can have the benefit of better generalization. Moreover, for very high resolution images (which is often the case for document images representing text) the cost of building the RL vectors from the original images is significantly higher than computing them on S3 or S4, especially if we use multi-layer pyramids.

We now analyze the performances related to different tasks and methods:

- Retrieval. We can see that KNN (and retrieval at top, not shown) performs extremely well in general for all datasets, while MAP performs rather poorly. As was discussed above, the good performance obtained with KNN (and P@5 not shown) is because for most documents we can find documents from the same class for which the similarity is high when using well designed RL features. As we found that in general P@1 is higher than KNN (except for NIT), we can conclude that using only a single example to classify the documents performs better than using $k = 4$ (fixed in our experiments). On the other hand, the poor MAP performance shows that there is a large within-class variation and it is difficult to retrieve all relevant documents using a single example. Indeed, for example in the case of MARG given a one column document from a class allows to retrieve easily the other one column documents from the same class but has difficulties to rank higher the two column documents from the same class than many of the one column documents from other classes. However, preliminary results have shown that metric learning approaches specifically designed to support KNN classification [13, 38] or ranking [6] can significantly improve the MAP in most cases.

- SVM. The discriminative linear classifier (SVM) even with a set of fixed parameter set ($\lambda = 1e-5$, $\rho = 5$, $N_i = 100$) yields to much better classification accuracy than NCM, showing that in the corresponding feature space nevertheless the classes are linearly separable. In the case of IH1 and clefIP the SVM results are better than nearest

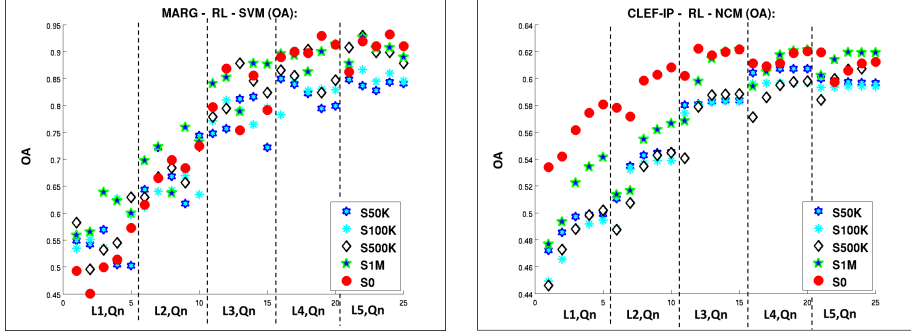


Figure 7: Examples images comparing different image resolutions.

neighbor search, but for MARG and NIT they remain below the KNN with $k = 1$. Note that IH1 and clefIP are much larger datasets than MARG and NIT, allowing the SVM to better learn the discriminative classifiers. Moreover, the poor SVM results for NIT is not surprising as several classes have very few examples to properly learn the linear classifier in these high dimensional spaces.

- NCM. Concerning the NCM classification, we made some tentatives to improve the NCM by replacing it with NCMC [26], but the number of optimal centroid per class varies a lot from one class to another and fixing the same number of centroids (*e.g.* 2 or 3) does not allow us to significantly improve the classification performance (except for MARG, where we have clear sub-classes according to the number of columns). KNN with $k = 1$ (P@1 results, not shown) is higher than with $k = 4$ (except for CLEF-IP) and SVM results shows rather good linear separability. This suggests that the documents within a class are not necessarily grouped around a few centroids but that they are rather scattered in the feature space.

Another way to improve the NCM classification performance is by using metric learning as proposed in [26], where the distances between the class means and the documents are computed in the space projected by a transformation matrix learned on the training set by maximizing the log-likelihood of the correct NCM predictions in the projective space (using a mini-batch stochastic gradient descend (SGD) with fixed learning rate $\lambda = 1$ and using 200 random batch of the size equal to the number of classes). Similarly to SVM, again we trained the NCM metric learning approach with the parameters below obtained as best on the XRCE dataset. This means that the results are suboptimal and we could improve the results further by tuning them on each tested datasets, which could be another option that was out of the scope of this paper.

Concerning the learned projected space, we experimented with different target dimensions D such as 16, 32, 64 and 128 and in Table 3 we show the best results obtained with the corresponding parameters. In addition, we also present the results when the projection was made using the D first principal directions⁹ of the PCA. In this set of experiments we only varied the number of layers in the pyramid, did no image rescaling (S0) and used $Q = 11$ quantization bins. We can see that while using PCA the results remain almost the same as without, the metric learning allows us to significantly improve the NCM performance in all cases. This time the NCN performance is close to the KNN and SVM performances, and could be further improved if we fine tune the

⁹Note that we initialize the metric learning with PCA.

W	MARG	IH1	NIT	CLEF-IP
I	61.8 (L5,D0648)	91.3 (L5,D10648)	59.8 (L5,D10648)	62.4 (L3,D1848)
PCA	61.4 (L5,D128)	91.3 (L5,D128)	59.6 (L5,D128)	62.1 (L3,D128)
ML	89(L5,D64)	92.6(L5,D64)	81.3(L5,Q11)	86.6(L5,D128)

Table 3: Comparison of the NCM results without projection ($\mathbf{W} = \mathbf{I}$), with PCA projections and with metric learning.

parameters on the tested dataset.

Note that the projected features are much smaller than the original features, especially for the multi-layer pyramid where for Q11 and L5 we go from 10648 to 128 dimensions, which can be interesting in case we want to store the features. We also experimented KNN and SVM with the PCA reduced features and we observed that, similarly to the NCM results, we were able to keep similar performances in all cases in spite of the strong dimension reduction. While similar observation was made in [15], Gordo *et al.* [18] proposes a compression and binarization through PCA embedding that significantly outperforms the results obtained with simple PCA.

4.2 Test different parameters for FV

Similarly to the previous section, we tested different parameter configurations for the Fisher Vectors (FV) built on local SIFT descriptors. To build the FV in natural images, first local patches (windows of size NxN) are extracted densely at multiple scales and SIFT descriptors are computed on each of them. For N we consider the values 24, 32, 48 and 64 and denote them by W1, W2, W3 and W4 respectively.

In the case of document images, especially when the images are of similar resolution, extracting features at multiple scales might have less importance, therefore in the first set of experiments we focus on extracting features only at a single scale. Also, as the resolution of most original images is very large and the considered local patches relatively small, we first resize the images¹⁰ to have a maximum of 250K pixels (S3). Then on each local window, we compute the usual 128 dimensional SIFT features [25], and reduce them to 48, 64 and 96 dimensions using PCA. We denote the corresponding low level features by F1, F2 and F3. While we can also build FV with the original SIFT features, we do not report results on it as we observed that reducing the dimensionality not only significantly decreases the size of the FV, but in general the accuracy is also improved.

In a given projected feature space, *e.g.* corresponding to W3 and F2, we build a set of visual vocabularies using Gaussian Mixture Model (GMM) with diagonal covariance matrices, where we vary the number of visual words by considering $2^{(g+3)}$ Gaussians where $g = 1..7$. We denote the corresponding vocabularies by G1..G7, where *e.g.* G1 corresponds to 16 Gaussians and G5 to 256 Gaussians. Note that both the PCA projection matrices and the GMM models were built using the features extracted on the XRCE dataset and then applied to all the other datasets. This means that for a given parameter setting (W,F,G) the documents are represented exactly in the same feature space (FV) independently of the dataset on which the experiments are done¹¹.

¹⁰When using FV with natural images we often resize the images first, often to 100K pixels [27, 29].

¹¹At the end of this section, to show the influence of the visual model, we provide a few results with the

	MARG	IH1	NIT	CLEF-IP
MAP	34.2 ± 0.3 W3,F1,G4	73.5 ± 0.2 W3,F2,G1	44.6 ± 1.5 W3,F2,G1	41.9 ± 0.1 W4,F1,G1
W	W3 (52/2)	W4 (71/9)	W4 (67/8)	W3 (42/4)
F	F1 (80/.8)	F1 (69/2)	F1 (61/.5)	F1 (75/2)
G	G1 (35/1)	G1 (70/6)	G1 (68/1)	G1 (98/9)
KNN	89.8 ± 1.3 W3,F1,G4	95.4 ± 0.3 W4,F1,G3	82.1 ± 2 W2,F1,G3	86.2 ± 1.1 W3,F1,G2
W	W3 (53/11)	W4 (100/6)	W2 (35/2)	W3 (41/9)
F	F1 (71/4)	F1 (84/2)	F1 (36/.8)	F1 (76/5)
G	G1 (32/6)	G1 (77/5)	G5 (37/1)	G1 (89/17)
NCM	69.1 ± 0.9 W3,F1,G5	91.6 ± 0.3 W3,F1,G4	77.8 ± 3 W1,F3,G7	69.9 ± 0.1 W3,F1,G1
W	W3 (95/4)	W3 (78/6)	W2 (55/7)	W3 (95/4)
F	F2 (37/1)	F1 (54/.3)	F3 (53/1)	F1 (64/2)
G	G7 (57/3)	G4 (37/.4)	G7 (88/6)	G1 (58/3)
SVM	87.4 ± 1 W4,F1,G4	97.3 ± 0.2 W3,F3,G6	85.7 ± 2.3 W2,F2,G6	87.6 ± 0.2 W3,F3,G6
W	W4 (86/4)	W3 (79/.3)	W3 (42/1)	W3 (100/2)
F	F1 (48/1)	F3 (54/.2)	F2 (37/1)	F3 (88/.8)
G	G6 (25/3)	G5 (55/.4)	G6 (27/4)	G7 (70/1)

Table 4: Comparative retrieval (MAP) and classification (KNN, NCM, SVM) results where we vary the size of the local window (W), the dimension of the PCA-reduced SIFT features (F) and the number of Gaussians used in the visual vocabulary (G) to build the FVs. We show best results in red (averaged over 5 splits) with the corresponding configuration in blue (below the accuracy), best parameter frequencies and performance variations per feature type.

In this first set of experiments, as we do not use any spatial pyramid, we have only three varying parameters for the FV: the size of the local window (W), the dimension of the PCA-reduced SIFT features (F) and the number of Gaussians used in the visual vocabulary (G). Retrieval (P@1, P@5 and MAP) and overall (OA) classification (with KNN, NCM and SVM) accuracies with the best parameter settings, winning frequencies and variances are shown in Table 4. From these results we can conclude the followings:

- Feature size: Best results are obtained in general with F1 (SIFT reduced to 48 dimensions) or, when it is not the case (*e.g.* NCM applied to NIT or SVM applied to CLEF-IP), the low average variances suggest that the corresponding results obtained with F1 are not very different.

- Vocabulary size. The number of Gaussians seems to be dependent both on the dataset and the tasks. In the case of retrieval, best results are obtained with smaller vocabulary sizes, and hence much smaller image signatures, most often G1 (except top retrieval on NIT). On the other hand, NCM and SVM seems to require much larger vocabularies, which is not surprising especially concerning SVM. We observe that, while extreme values (G1 or G7) yield often best or worse results, using values between 64

visual vocabulary built on the same dataset on which the experiments were performed.

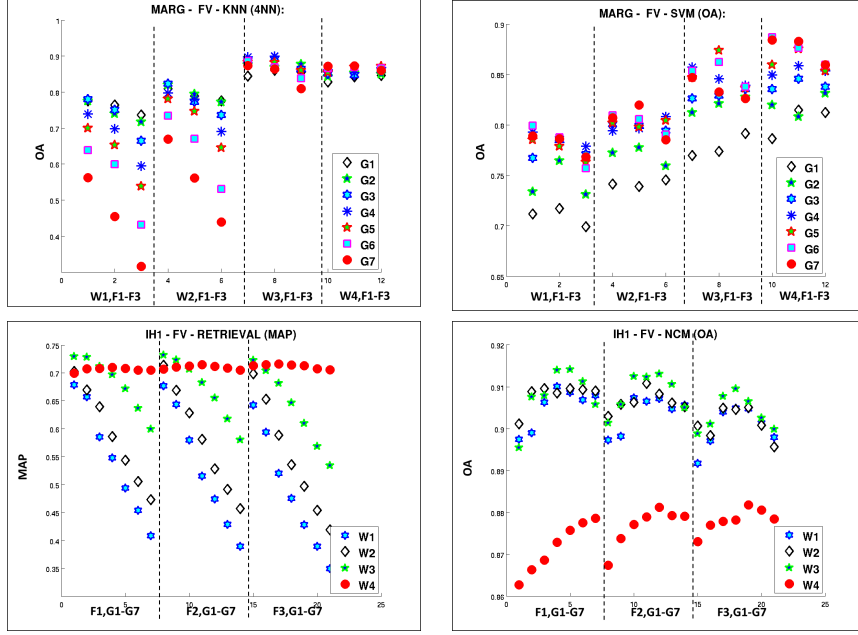


Figure 8: Example plots comparing different vocabulary sizes (top) and window sizes (bottom).

(G3) and 256 (G5) seems to be a good compromise between size and accuracy (see also Figure 8, top row).

- Window size: W3 (patches of size 48x48) seems to be often best performing or a good compromise compared to the other cases. Indeed, W1 performs in general poorly showing that a too small window (containing rather few information about the page) is not a good idea. While W4 can perform best for certain tasks (*e.g.* retrieval on Bytel) it can be worse on another task (NCM on Bytel), as shown in Figure 8, bottom row. The variances are also high, showing the importance of setting this parameter properly.

Note nevertheless that the ideal size of the window is strongly correlated with the processed image size. If we increase the image size we need larger windows to capture the same amount of information. Decreasing the image while keeping the same window size allows to increase the amount of information per windows. Another possibility to ensure we capture the information at the right scale is to extract the features at multiple scale. Therefore in which follows we vary both the image size and the number of scales at which the features are extracting, while fixing the window size to 48x48 (W3).

As we observed that S1 (50K) performs in general poorly, we consider the following image sizes: 100K (S2), 250K (S3) and 500K (S4) pixels respectively. Note that we do not consider S0 and S5 (1M pixels) as they lead not only to extremely large amount of windows (increasing significantly the computational cost), but also the information captured within such window is extremely poor in content (many of them containing only white pixels). As we have seen that W1 on S3 (containing much less information than W3) performed poorly, we expect even worse results when using W3 with S0 or S5. To get similar or possible better results one might consider much larger windows

RET	MARG	IH1	NIT	CLEF-IP
MAP	35.3 \pm 0.1 S3,M5,G5	75.7 \pm 0.2 S3,M3,G2	46.6 \pm 1.5 S3,M5,G1	46.1 \pm 0.8 S2,M7,G2
S	S3 (64/.9)	S3 (68/5)	S3 (89/1)	S2 (69/2)
M	M5 (76/.9)	M7 (57/4)	M5 (81/.7)	M7 (88/3)
G	G5 (63/.9)	G1 (65/6)	G1 (83/2)	G1 (78/3)
KNN	91.4 \pm .9 S3,M7,G3	95 \pm 0.2 S3,M3,G1	81.7 \pm 2 S4,M7,G5	89.9 \pm 0.8 S4,M7,G2
S	S3 (81/3)	S3 (87/2)	S4 (68/2)	S4 (94/4)
M	M5 (57/2)	M5 (44/1)	M5 (38/.9)	M7 (43/4)
G	G4 (33/2)	G1 (85/4)	G3 (25/1)	G1 (49/5)
NCM	71.2 \pm 1.6 S3,M7,G6	92.2 \pm 0.2 S3,M3,G5	75.2 \pm 2.1 S4,M3,G7	75.9 \pm 0.3 S2,M5,G5
S	S3 (59/2)	S3 (53/.9)	S4 (43/3)	S2 (86/2)
M	M5 (60/2)	M3 (44/.5)	M1 (81/2)	M5 (49/3)
G	G5 (58/4)	G4 (42/.7)	G7 (58/4)	G1 (27/1)
SVM	91 \pm 1.1 S4,M7,G5	97.4 \pm 0.1 S4,M7,G7	86.5 \pm 2.1 S3,M3,G4	94.7 \pm 1.1 S4,M7,G7
S	S3 (57/2)	S3 (64/.4)	S3 (64/1)	S4 (93/1)
M	M5 (45/2)	M5 (63/.3)	M3 (38/.6)	M5 (57/2)
G	G5 (58/3)	G7 (51/.4)	G5 (50/1)	G7 (88/1)

Table 5: Comparative FV results on different datasets and tasks. We show best results in red and best parameter settings in blue using different evaluation measures.

to compute the SIFT features.

To handle the feature extraction at multiple scale we further downscale the image (*e.g.* S3) by a scale factor of $\sqrt{2}$ and extract SIFT again from windows of size 48x48. The amount of information in these windows extracted from the image downsampled by $\sqrt{2}$ corresponds to the (smoothed) information extracted from S3 with a window W3 upscaled by $\sqrt{2}$. We repeat this process until which we reach the number of desired scales. We experimented with 1,3,5 and 7 scales denoting them by M1, M3, M5 and M7. Note that in the case of the configuration (S3,W3,M5) this means that the images of size S3 were 5 times downsampled by $\sqrt{2}$ and at each scale the SIFT features were extracted on windows of size 48x48. These features are PCA-reduced to a dimension of 48 (F1) and all cumulated to form the feature set X_I that generates the FV corresponding to the image.

The result with varying number of scales (M), image resolutions (S) and vocabulary sizes (G) are shown in Table 5. From these results, we can conclude the followings:

- Number of scales. Concerning the number of scales (M), extracting features at multiple levels definitely helps. While there is no clear winner between M3, M5 and M7, as the plots in Figure 9 top row shows they have similar performances and in general all outperform M1. This suggest that while it is important to consider multiple scales, considering 3 or 5 scales, are in general, sufficient.

- Vocabulary size. The behavior of the visual vocabulary size remains similar to our previous set of experiments where we varied the window size (W) and the feature dimension (F). Again, while extreme values (G1 or G7) are often best or worst, G3,

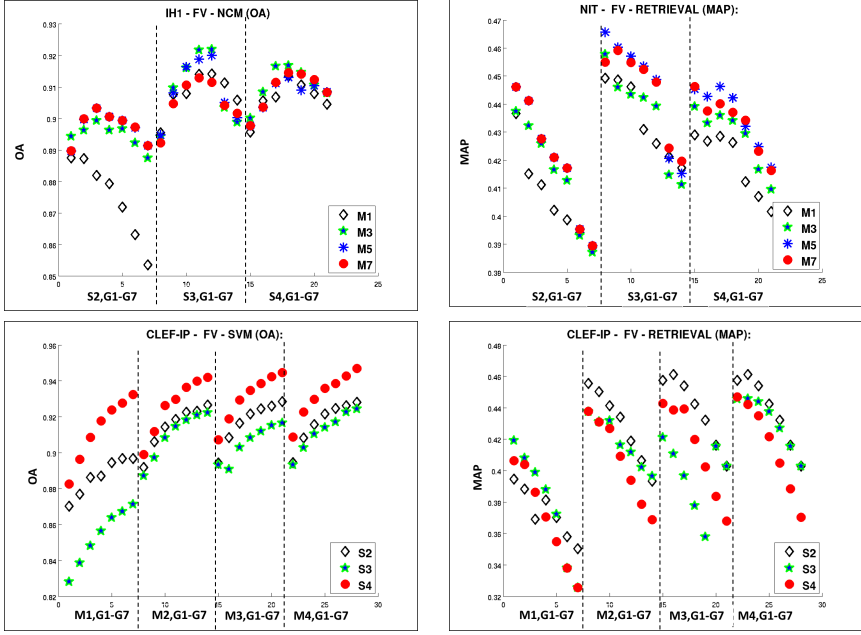


Figure 9: Example plots comparing different number of scales (top) and image sizes (bottom).

G	G1	G2	G3	G4	G5	G6	G7
L	5	5	4	3	3	2	2
Nb reg	121	121	57	21	21	5	5
FD	185856	371712	350208	258048	516096	245760	491520

Table 6: A summary of the feature sizes

G4 and G5 are often close to best or even winning in the case of MARG where G5 performs the best on all tasks.

- Image size. S3 (250K pixels) is the best performing in most cases with MARG and IH1, showing that the configuration (S3,W3) is suitable for them. Concerning NIT and CLEF-IP, there is no clear winner (see also Figure 9, bottom rows). For nearest neighbor search based methods (KNN, P@1,P@5) and SVM when using window size of W3 it seems better to keep higher resolution (S4) while retrieval and NCM classification on CLEF-IP works better with low resolution (S2).

Finally, we test the spatial pyramid with several layers for the FV features, where we consider the number of maximum layer in the pyramid in function of the visual vocabulary as FV features being already very large for vocabulary sizes above 64 to obtain the final signature size they are multiplied by the number of regions in the pyramid. We show in Table 6 the maximum number of layers we consider for each vocabulary size in our experiments. We also show the number of corresponding regions and the size of the final signature (after the concatenation of the FVs for all the regions).

We can see that these signatures are very large and in general not sparse and we

	MARG	IH1	NIT	CLEF-IP
P@1	95.1/95.1 S3,L2,G4	95.2/94.5 S3,L2,G1	83.3/81.7 S4,L2,G4	89/87.9 S4,L1,G1
P@5	83.1/83.1 S3,L2,G5	93.8/92.9 S3,L2,G1	75.9/74.9 S4,L3,G4	86/84.6 S4,L1,G1
MAP	36.2/36.2 S3,L2,G5	76.5/75.4 S3,L2,G1	46.6/41.6 S4,L4,G1	46.1/42.1 S2,L1,G1
KNN	93.1/93.1 S3,L2,G3	95/94.2 S3,L2,G2	82.8/81.9 S4,L3,G4	89.6/88.1 S4,L1,G1
NCM	75/72.4 S3,L5,G2	92.4/92.4 S3,L3,G1	78.3/75.8 S4,L3,G5	76.1/75.1 S2,L4,G1
SVM	92.5/90.7 S3,L4,G3	97.4/97.2 S4,L1,G7	86.5/84.9 S3,L1,G4	95.5/93.5 S4,L2,G6

Table 7: Comparative FV results on different datasets and tasks. We show best results (red) versus result using fixed parameter settings (blue) where we used (S3,L2,G4) for MARG and IH1, (S4,L2,G4) in the case of NIT and (S4,L1,G4) for CLEF-IP. We also show the parameter setting that provided the best results.

did all our experiments with non-compressed FVs. Note nevertheless that there are several methods in the literature [28, 33, 16, 37] that propose to efficiently binarize and/or compress the Fisher Vectors while keeping them highly competitive. It could be interesting, but testing the effect of methods in the case of different configurations was out of the scope of the paper.

In Table 7 and Figure 10 we show results when we vary the image size, the number of pyramid layers and the number of Gaussians and fix the other parameters to W3, F1 and M5. Analyzing the results suggest that while the best configuration varies a lot, in general we get best results with relatively few layers or even a single one and often only with few Gaussians.

Spatial pyramid. If we analyze these results in more details, we can see that only NCM and SVM on MARG performed best with 5 and 4 layers respectively. In general, it seems that NCM was the one that took the most advantage from more than 2 layers. In the case of SVM what is beneficial is large signatures (which is not surprising), but using fewer layers with larger vocabularies seems to perform better than smaller vocabularies with more layers. This is somewhat in contrast to what we observed for RL and the results in [23] concerning spatial pyramids with FVs on natural images.

In Table 7 we also show results (in blue) for each dataset given a fixed configuration found as reasonably close to best results on most tasks. These configurations are (S3,L2,G4) for MARG and IH1, (S4,L2,G4) in the case of NIT and (S4,L1,G4) for CLEF-IP, where we have in addition (W3,F1,M5) for all datasets. We can see that in most cases these fixed values are indeed good choices, except for CLEF-IP for which it is less obvious to find a good set of configurations, especially concerning the image size that performs well on all tasks (as shown also Figure 9, bottom row). This is probably due to the fact that in this dataset the size of the images is extremely variable. The best compromise we found was S4, G4 without spatial pyramid (L1), however the drop in accuracy is more important than for the other datasets.

Finally, to show the influence of the visual model, we rerun the last set of experiments, but instead of using the visual models built on the XRCE dataset, for each

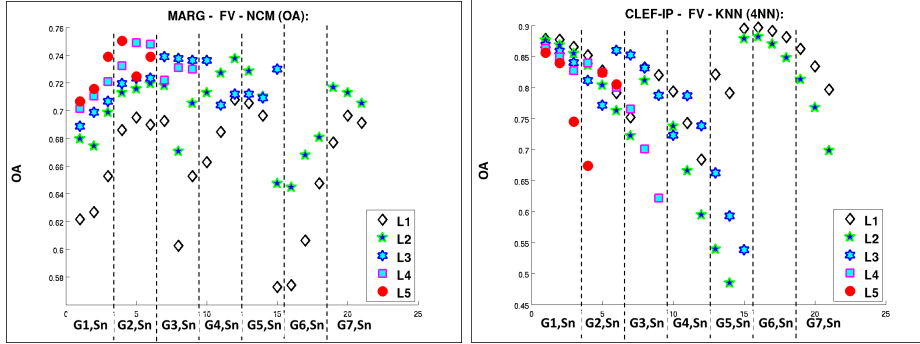


Figure 10: Examples plots comparing different pyramid layers.

	MARG	IH1	NIT	CLEF-IP
P@1	95.9/95.1 S3,L5,G1	95.4/95.2 S4,L2,G1	82.5/83.3 S4,L2,G3	87.7/89 S4,L1,G1
P@5	85/83.1 S4,L4,G2	94/93.8 S4,L2,G1	75.4/75.9 S4,L3,G2	84.7/86 S4,L1,G1
MAP	37.8/36.2 S3,L4,G2	76.6/75.4 S4,L2,G1	45.8/46.1 S4,L4,G1	42.8/46.1 S2,L1,G1
KNN	95/93.1 S3,L3,G2	95.3/95 S4,L3,G1	82.8/82.8 S4,L3,G2	88.8/89.1 S4,L1,G1
NCM	81.1/75 S2,L3,G4	92.6/92.4 S4,L3,G1	78.7/78.3 S4,L4,G1	75.7/76.1 S2,L4,G1
SVM	94.1/92.5 S4,L5,G2	97.4/97.4 S4,L2,G7	86.5/86.5 S3,L1,G4	95.8/95.5 S4,L2,G6

Table 8: FV results when the visual models were built SIFT features extracted from the images of the tested dataset (red) and compared with the visual model on XRCE (blue). We also show the parameter setting that provided the best results for the results obtained with the visual models trained on the dataset itself.

dataset we trained its own model with the SIFT features extracted from the training images of the tested dataset. The results in Table 8 show on one hand that we do not have a clear winner between the two models. On the other hand while the best configuration per dataset and task varies, the best score obtained are often close. This show somewhat that the data on which the vocabulary is built has relatively little influence on the results the moment we use the images that have similar content which is the case for document images.

4.3 Combine RL with FV

The most natural way to combine RL and FV is early or late fusion. As we use dot product for retrieval, the dot product of the concatenated features (early fusion) is equivalent to the sum of the dot products (late fusion). Similarly, the NCM centroids of the concatenated features are the concatenation of the RL respectively FV centroids, and from therefore late and early fusion are again equivalent.

To test the late fusion of RL with FV, we consider the configuration (S0,L5,Q11) for RL and the fixed parameters settings leading to the values in blue in the Table 7 for FV.

	signature	MARG	IH1	NIT	CLEF-IP
MAP	RL	33.2	64.3	38.5	35.6
	FV	36.1	75.4	41.6	42.1
	RL+FV	36.5	76.9	44.2	48.2
KNN	RL	89.9	93.1	76.7	80.8
	FV	92.6	94.2	81.9	88.1
	RL+FV	93	95.2	80.2	91.1
NCM	RL	63.2	91.3	65.6	61.2
	FV	72.4	92.4	75.8	75.1
	RL+FV	73.4	93	79.8	75.8
SVM	RL	91.9	96.7	78.2	89.5
	FV	90.7	97.2	84.9	93.5
	RL+FV	92.8	97.7	83.7	94.4

Table 9: Results with late fusion of RL and FV features on different datasets and tasks.

The results obtained are shown in Table 9. We can see that even with a simple equally weighted late fusion, in general (except for NIT) we obtain significant improvements both on retrieval and classification.

We would like to mention here another possible combinations of the RL with FV where the main idea is to consider the RL features as low level features (replacing the SIFT) such that on each local window we build a RL histogram. Then the visual vocabulary (GMM) and the FV are built with these local RL features directly or as some PCA reduced forms of them. Note also that if we use small image patches, the number of quantization of the runs (Q) can be reduced as anyway a run cannot be longer than the patch size. We intend in the future to explore if such FVs on RL performs better than the global RL features and also if combining all three signatures can further improve the accuracy.

5 Image-based Patent Retrieval

We would like first to recall briefly our participation in the Image-based Patent Retrieval task's at Clef-IP 2011 [30]. A more detailed description especially concerning the text representation and retrieval can be found in [11]. The aim of the challenge was to rank patents as relevant or non relevant one given a query patent while using both visual and textual information. There were 211 query patents provided and the collection to search in contained 23444 patents having an application date previous to 2002. The number of images varied a lot, from few images to several hundred of images per patent. In total we had 4004 images in the query patents and 291,566 images in the collection. As image representation we used the FV with the configuration (S3, W2, F2, G5 and L1) where the model (PCA and GMM) were trained on CLEF-IP, *i.e.* the training set of the Image Classification Task of Clef-IP 2011 [30]. The similarity between images was given by the dot product of two Fisher Vectors.

We tested two main strategies. In the first case, we considered the average distance between all pairs of images given two patents with the corresponding set of images (MEAN). In the second case we considered only the maximum of all similarities computed between pairs of images (MAX).

We also considered to integrate in the system our automatic image-type classifier (using the same FV features) that was trained on the CLEF-IP dataset and we used it

Table 10: Image-based Patent Retrieval: overview of the performances of our different approaches. The performances are all shown in percentages.

Model /strategy	MEAN			MAX		
	ID	MAP	P@10	ID	MAP	P@10
Classifier						
not used	I1	0.56	0.20	I2	1.84	0.75
class means	I3	0.80	0.40	I4	1.84	0.70
only drawings	I5	1.09	0.62	I6	3.51	1.85

to predicted the image type. Using the predicted scores we considered the similarities between class means (averaging the images predicted to belong to a given class), and took the average or the maximum according to the strategy considered.

Finally, as in the considered patent classes (A43B patents related to footwear, A61B patents concerning diagnoses and surgery and H01L patents proposing new semiconductor and electric solid state devices) the drawings were the most relevant images, we discarded all images not predicted as drawings and computed the mean or max similarities between the images predicted as drawings. Note that for other patent classes, considering images containing chemical structures or gene sequences would be more appropriate.

The results detailed in [11] are recalled in Table 10. They show that the max strategy is better than considering average similarities. Considering class means instead of global mean improves the MEAN strategy, but has no effect on the max strategy. Finally, considering only drawings performed the best for both strategies.

While all these retrieval accuracies are very low, we want to make a few remarks. First, the task was really challenging as relevant prior art patents do not necessarily contain images similar to relevant images in the query patent. Second, even with this poor image based ranking and simple late fusion we were able to improve the text only based patent ranking especially with the I5 strategy (see details in [11]). Third, we can use more complex fusion methods to merge visual and textual retrieval (see *e.g.* the graph based methods described in [3]).

On the other hand the image type classification can also be improved in several ways. On one hand we can select better feature configuration for FV combined with RL features as above or even using some new, deep convolutional neural networks (CNNs) based representations such as in [21, 19].

Second, the strategies to consider and combine features from set of images in [11] was rather simple. Instead, we can see the set of patent images as a multi-page document and use the methods proposed in [17, 15, 32] to handle classification and retrieval with multi-page documents.

For example, the bag-of-pages model of [17], consider PCA-reduced RL features for each page and build a FV for the document, *i.e.* when computing FV with Eq. 4, the features \mathbf{x}_t corresponds to the RL features computed for the pages in the document page. Similarly, we can build a FV with the RL features built on the patent images, and represent the patent containing these images with the obtained FV. Then two patents are compared with the dot product of these FVs.

In [15] the bag-of-classemes was proposed and have been shown to outperform the bag-of-pages. In this case the \mathbf{x}_t features are the image type classification scores concatenated into a single vector (called classeme) and the FV is built on top of these

vectors. Note nevertheless, that while in [15] the bag-of-classemes outperforms the bag-of-pages, the addressed problem is different, *i.e.* document classification. In addition all pages have the same class label, the one inherited from the document. In our case, in a patent we have different image types and therefore we could describe by bag-of-classemes the distribution of different type of images within a patent. While this can be a useful information for the patent expert, it does not necessarily improves for example patent prior art search.

Finally, we can also improve the image type classification by combining the visual information with information from text. Text can come from the patent, if we can access image caption and/or the paragraphs where the image is referred. The extracted text can be represented by bag-of-words that can be used to train classifiers which learn implicitly which words are relevant to discriminate image types. The textual and visual classifiers can after be merged at score level (late fusion). Alternatively, we can consider embedding both the visual and textual features in the same subspace using CCA and train a classifier in the embedded space as in [14]. Note that text information can also be extracted from the document image using OCR. In the case of patent images, using bag of "n-grams of characters" on the text extracted from the image content could be more appropriate than bag-of-words to describe for example gene sequences, mathematical formulas and chemical structures.

6 Conclusion

In this paper we made an exhaustive experimental study on RunLength Histogram (RL) and Fisher Vector (FV) based representations for document image classification and retrieval. We compared different parameter configurations for both features using several datasets, methods and evaluation methods. We designed suitable configurations for both features and while they might be suboptimal for individual tasks, features designed with the proposed configurations are reasonable in case one might want to solve different tasks with the same features. Then we discussed the usage of patent images in prior art search as such an example.

References

- [1] The Medical Article Records Groundtruth Dataset. <http://marg.nlm.nih.gov/roverintro.asp>.
- [2] The NIST Structured Forms Database (NIST Special Database 2). <http://www.nist.gov/ts/msd/srd/nistsd2.cfm>.
- [3] Julien Ah-Pine, Gabriela Csurka, and Stephane Clinchant. Unsupervised visual and textual information fusion in cbir using graph-based methods. *ACM Transactions on Information Systems*, 33(2), 2015.
- [4] Zeynep Akata, Florent Perronnin, Zaid Harchaoui, and Cordelia Schmid. Good practice in large-scale learning for image classification. *PAMI*, 36:507–520, 2014.
- [5] A.D. Bagdanov and M. Worring. Multiscale document description using rectangular granulometries. *International Journal on Document Analysis and Recognition*, 2003.

- [6] Bing Bai, Jason Weston, David Grangier, Ronan Collobert, Kunihiko Sadamasa, Yanjun Qi, Olivier Chapelle, and K.Q. Weinberger. Supervised semantic indexing. In *CIKM*, 2009.
- [7] L. Bottou. Large-scale machine learning with stochastic gradient descent. In *COMPSTAT*, 2010.
- [8] Yung-Khan Chan and Chin-Chen Chang. Image matching using run-length feature. *Pattern Recognition Letters*, 22:447–455, 2001.
- [9] Nawei Chen and Dorothea Blostein. A survey of document image classification: problem statement, classifier architecture and performance evaluation. *IJDAR*, 10:1–16, 2007.
- [10] G. Csurka, C. Dance, L. Fan, J. Willamowski, and C. Bray. Visual categorization with bags of keypoints. In *ECCV Workshop on Statistical Learning for Computer Vision*, 2004.
- [11] Gabriela Csurka, Jean-Michel Renders, and Guillaume Jacquet. XRCEs participation at patent image classification and image-based patent retrieval tasks of the Clef-IP 2011. In *Intellectual Property Evaluation Campaign (CLEF-IP)*, 2011.
- [12] J. F. Cullen, J.J. Hull Jonathan, and P.E. Hart. Document image database retrieval and browsing using texture analysis. In *ICDAR*, 1997.
- [13] Jason V. Davis, Brian Kulis, Prateek Jain, Suvrit Sra, and Inderjit S. Dhillon. Information-theoretic metric learning. In *ICML*, 2007.
- [14] A Gordo, F Perronnin, and E Valveny. Document classification using multiple views. In *DAS*, 2012.
- [15] Albert Gordo. *Document Image Representation, Classification and Retrieval in Large-Scale Domains*. PhD thesis, Computer Vision Center, Universitat Autònoma de Barcelona, 2013.
- [16] Albert Gordo and Florent Perronnin. Asymmetric distances for binary embeddings. In *CVPR*, 11.
- [17] Albert Gordo and Florent Perronnin. A bag-of-pages approach to unordered multi-page document classification. In *ICPR*, 2010.
- [18] Albert Gordo, Florent Perronnin, and Ernest Valveny. Large-scale document image retrieval and classification with runlength histograms and binary embeddings. *Pattern Recognition*, 46(7):1898–1905, 2013.
- [19] Adam Harley, Alex Ufkes, and Konstantinos Derpanis. Evaluation of deep convolutional nets for document image classification and retrieval. In *ICDAR*, 2015.
- [20] Pierre Heroux, Sébastien Diana, Arnaud Ribert, and Eric Trupin. Classification method study for automatic form class identification. In Proceedings of the International Conference on Pattern Recognition, 1998, 1998.
- [21] Le Kang, Jayant Kumar, Peng Ye, Yi Liy, and David Doermann. Convolutional neural networks for document image classification. In *ICPR*, 2014.

- [22] Daniel Keysers, Faisal Shafait, and Thomas M. Breuel. Document image zone classification - a simple high-performance approach. In *CVPR*, 2007.
- [23] Josip Krapac, Jakob Verbeek, and Frédéric Jurie. Modeling spatial layout with fisher vectors for image categorization. In *ICCV*, 2011.
- [24] S. Lazebnik, C. Schmid, and J. Ponce. Beyond bags of features: spatial pyramid matching for recognizing natural scene categories. In *CVPR*, 2006.
- [25] D. Lowe. Distinctive image features from scale-invariant keypoints. *IJCV*, 60(2):91–110, 2004.
- [26] Thomas Mensink, Jakob Verbeek, Florent Perronnin, and Gabriela Csurka. Distance-Based Image Classification: Generalizing to new classes at near-zero cost. *IEEE PAMI*, 35(11):2624–2637, November 2013.
- [27] F. Perronnin and C. Dance. Fisher kernels on visual vocabularies for image categorization. In *CVPR*, 2007.
- [28] F. Perronnin, Y. Liu, J. Sánchez, and H. Poirier. Large scale image retrieval with compressed fisher vectors. In *CVPR*, 2010.
- [29] F. Perronnin, J. Sánchez, and Thomas Mensink. Improving the fisher kernel for large-scale image classification. In *ECCV*, 2010.
- [30] Florina Piroi, Mihai Lupu, Allan Hanbury, and Veronika Zenz. CLEF-IP 2011: Retrieval in the Intellectual Property Domain. In *Intellectual Property Evaluation Campaign (CLEF-IP)*, 2011.
- [31] I. Pratikakis, B. Gatos, and K. Ntirogiannis. Icfhr 2012 competition on handwritten document image binarization. In *ICFHR*, 2012.
- [32] M. Rusnol, V. Frinken, D. Karatzas, A. D. Bagdanov, and J. Lladós. Multimodal page classification in administrative document image streams. *IJDAR*, July, 2014.
- [33] J. Sanchez and F. Perronnin. High-dimensional signature compression for large-scale image classification. In *CVPR*, 2011.
- [34] Prateek Sarkar. Image classification: Classifying distributions of visual features. In *ICPR*, 2006.
- [35] Christian Shin, David Doermann, and Azriel Rosenfeld. Classification of document pages using structure-based features. *IJDAR*, 2001.
- [36] J. Sivic and A. Zisserman. Video google: A text retrieval approach to object matching in videos. In *ICCV*, volume 2, pages 1470–1477, 2003.
- [37] A. Vedaldi and A. Zisserman. Sparse kernel approximations for efficient classification and detection. In *CVPR*, 2012.
- [38] K. Weinberger and L. Saul. Distance metric learning for large margin nearest neighbor classification. *JMLR*, 10:207–244, 2009.